Evaluation of Globally Gridded Precipitation Data and Satellite-Based Terrestrial Water Storage Products Using Hydrological Drought Recovery Time

5 Çağatay Çakan[1], M. Tuğrul Yımaz[1], Henryk Dobslaw[2], E. Sinem Ince[3], Fatih Evrendilek[4], Christoph Förste[3], Ali Levent Yagci[5]
[1]Department of Civil Engineering, Water Resources Laboratory, Middle East Technical University, Ankara 06690, Turkey
[2]Section 1.3: Earth System Modeling, GFZ German Research Centre for Geosciences, Potsdam 14473, Germany
[3]Section 1.2: Global Geomonitoring and Gravity Field, GFZ German Research Centre for Geosciences, Potsdam 14473, Germany
10 [4]Department of Civil and Environmental Engineering, University of Maine, Orono, Maine 04469, USA
[5]Department of Geomatics Engineering, Gebze Technical University, Kocaeli 41400, Turkey

Correspondence to: Çağatay Çakan (cakan.cagatay@metu.edu.tr)

Abstract. Accurate precipitation observations are crucial for understanding meteorological and hydrological processes. Most precipitation products rely on station-based observations, either directly or for bias correcting satellite retrievals. To validate

15 these station-based precipitation products, additional independent data sources are necessary. This study aims to assess the performance of the Global Precipitation Climatology Center (GPCC) Full Data Monthly Product v2022 and Global Precipitation Climatology Project (GPCP) v3.2 Monthly Analysis Product by estimating hydrological drought recovery time (DRT) from precipitation and terrestrial water storage anomaly (TWSA) acquired from satellite gravimetry. This study also evaluates the performance of G3P and JPL mascon Total Water Storage (TWS) monthly-solutions from the Gravity Recovery

20 and Climate Experiment (GRACE) and GRACE Follow-On (GRACE-FO) satellite missions. The current study employed two methods to estimate DRT and evaluated the consistency of DRT estimations by calculating the time difference between the two methods. No significant differences in the mean DRT estimations using GPCC and GPCP were found for both globally and across all climate zones, with comparable consistencies from GPCC and GPCP. For TWS products, DRT estimations using JPL mascon were, on average, 2.6 months longer than that using G3P. However, the G3P showed approximately 5.0%

25 higher consistency than the JPL mascon globally and across each climate zone. These results indicated a close agreement between GPCC and GPCP in DRT estimations. G3P showed greater consistency in DRT estimation with the precipitation products than JPL mascon. These findings provide valuable insight into accuracy of precipitation and TWSA products by utilizing hydrological drought characteristics, enhancing our understanding of meteorological and hydrological processes.

1 Introduction

30 Precipitation is a pivotal element in the global water cycle. It provides freshwater to continental regions and thereby allows vegetation to flourish. Average precipitation amounts and the associated temporal distribution of rain events characterize

climate zones and terrestrial ecosystems (Bayar et al., 2023; Lai et al., 2018). Too much or too little precipitation than usual, however, can have very severe impacts on biosphere, agriculture, and human societies in general. The close monitoring of droughts (Barker et al., 2016; Lai et al., 2019; Wu et al., 2023; Xu et al., 2015) and floods (Belabid et al., 2019; Harris et al.,

35   2007; Maggioni & Massari, 2018), as well as the prediction of precipitation at short, medium and long forecast horizons (Akbari Asanjan et al., 2018; Senocak et al., 2023) are a central objective of hydrometeorologic research.

In situ observations from rain gauges are typically utilized to monitor precipitation (Barker et al., 2016; Wehbe et al., 2017; Wei et al., 2019). However, the distribution of gauge stations is often sparse and uneven, particularly over complex terrains

40   where stations may be difficult to install and maintain (Wang et al., 2017). In contrast, satellite and satellite blended based precipitation products derived from remote sensing instruments have made essential strides, offering varying spatiotemporal resolutions as a viable alternative to ground-based observations (Bai et al., 2019; Prakash et al., 2015; Wang et al., 2017; Wu et al., 2023). The Global Precipitation Climatology Center (GPCC) and Global Precipitation Climatology Project (GPCP) are frequently used precipitation products with global coverage (Adler et al., 2003; Sun et al., 2018). GPCC represents ground-

45   based precipitation observations, whereas GPCP is a combination of satellite and in situ station observations.

Products from both GPCC and GPCP have been frequently compared with each other and against a wide range of atmospheric reanalyses (e.g., Prakash et al., 2015). At regional scales, particularly in the tropics, good agreement has been observed between GPCC and GPCP (Negrón Juárez et al., 2009; Sun et al., 2018). Moreover, the spatial distribution of annual and seasonal

50   rainfall climatology across West Africa was found to be consistent between GPCC and GPCP (Lamptey, 2008). Although there are regional similarities, there are also distinct differences. GPCC outperformed GPCP against station-based precipitation data in China (Wang et al., 2017), demonstrated enhanced spatiotemporal representativeness of precipitation patterns in Iran (Darand & Khandu, 2020), and showed superior performance in the Sahel region based on statistical error metrics (Ali et al., 2005). In general, these studies evaluate precipitation products by comparing them with in-situ observations. However, given

55   both datasets utilize ground station-based observations, indecency of the evaluation analyses becomes an important aspect. Accordingly, additional independent assessments may be needed for precipitation products that utilize observations such as GPCC and GPCP.

Drought monitoring is crucial since drought is one of the most destructive disasters, resulting from a significant decrease in a

60   region's water resources over an extended period. It can have disastrous consequences for ecosystems, human health, agriculture, irrigation, and water supply (AghaKouchak et al., 2015; Ding et al., 2020; Mishra & Singh, 2010; Patz et al., 2014; Piao et al., 2010). Drought indices, such as the standardized precipitation index (SPI, Mckee et al., 1993) and the standardized precipitation evapotranspiration index (SPEI, Vicente-Serrano et al., 2010), the standardized runoff index (SRI, Shukla & Wood, 2008) and the standardized streamflow index (SSI, Vicente-Serrano et al., 2012) are utilized to characterize drought

65   characteristics (e.g., frequency, severity, and recovery time). Meteorological droughts arise from insufficient precipitation,

whereas hydrological droughts result from insufficient water storage (Behrangi et al., 2015; Keyantash & Dracup, 2002; Thomas et al., 2014). SPI focuses solely on precipitation data, while SPEI utilizes precipitation and evapotranspiration data. SSI hinges on runoff yield from the land surface, while SRI utilizes streamflow in river channels (Lai et al., 2019). Complex hydrological models utilize precipitation data for hydrological drought assessment based on SSI and SRI (Lai et al., 2018;

70 Madadgar & Moradkhani, 2014). Alternatively, the water storage deficit can provide insights into hydrological drought without employing elaborate hydrological models (Thomas et al., 2014). It only requires measurements of the amount of water stored at or underneath the ground and is employed in the estimation of drought recovery time (DRT). By combining precipitation and terrestrial water storage (TWS) observations it is even possible to predict the amount of precipitation that will be required to re-fill any storage deficit (Singh et al., 2021).

75

The satellite mission Gravity Recovery and Climate Experiment (GRACE) provides such measurements of TWS (Springer et al., 2017). GRACE was conducted jointly by the National Aeronautics and Space Administration (NASA) and the German Aerospace Center (DLR) from 2002 until 2017. Since 2018, GRACE Follow-On (GRACE-FO), successor of GRACE, is operated by NASA together with the German Research Centre for Geosciences (GFZ) to further extend the data record until

80 present. Terrestrial water storage anomalies (TWSA), encompassing all subsurface and surface water balance components, are obtained by measuring tiny irregularities in the orbits of two identical twin-satellites that are trailing each other with a distance of roughly 200 km in polar orbit of initially 490 km altitude (Wahr et al., 2004). Temporal changes in the Earth's gravity field are computed from the comparison of observations from different times. Once atmospheric, oceanic and geophysical effects are removed, the remaining signal on monthly-to-interannual scales reflects variations in TWS. The ready-to-use TWS data

85 from GRACE and GRACE-FO missions are made available either as spherical harmonic (SH) or mass concentration solutions (mascons). GRACE-based TWS has been used in the past to relate interannual variations in TWS to large-scale climate modes (Pfeffer et al., 2023), and to validate hydrological models (Döll et al., 2024). There were even attempts to assimilate GRACE data into land-surface schemes (Eicker et al., 2014; Tangdamrongsub et al., 2021). Hence, GRACE and GRACE-FO are currently the most used datasets in global TWS.

90

The use of GRACE and GRACE-FO TWS products could be used for an independent assessment of precipitation products by drought monitoring, serving as an alternative to assessments conducted with hydrological models (Beck et al., 2017; Gebrechorkos et al., 2024). Existing studies evaluate precipitation products using drought monitoring and focus on drought indices such as SPI and SPEI (Golian et al., 2019; Wei et al., 2019, 2021). However, more independent assessment studies

95 using key parameters that encompass all subsurface and surface water balance components, such as TWS, are necessary to better understand the utility of precipitation products. This is particularly important for hydrological drought assessment, as spatial variability across different climate zones globally is still inadequately explored.

The current study aims to independently evaluate and compare frequently used global gridded precipitation products (i.e., GPCC and GPCP) by using the GRACE/GRACE-FO TWS data (i.e., the JPL mascon and G3P products) in order to assess drought conditions. Also, this research evaluates the performance of the JPL mascon and G3P TWS products. Both evaluation conducted by estimating DRT based on TWSA and required precipitation amount. Comparing the suitability of these precipitation and TWS products for global hydrological applications across various Köppen-Geiger climate zones enhance our understanding of the relationship between hydrological droughts and global precipitation and TWS products through DRT estimations.

2 Methodology

2.1 Datasets

2.1.1 GPCC and GPCP Precipitation

Established in 1989 by the World Meteorological Organization (WMO), the Global Precipitation Climatology Center (GPCC) integrates monthly land precipitation data from various sources including the global telecommunication systems (GTS), synoptic weather reports (SYNOP), and monthly climate reports (CLIMAT). GPCC offers different precipitation products with varying spatiotemporal resolutions, such as the Full Data Monthly Product (GPCC FDM), the Monitoring Product, and the First Guess Monthly Product. Given its suitability for model verification and water cycle studies, this study utilized GPCC FDM v2022 (Schneider et al., 2022) to analyze the relationship between precipitation and TWS (Schneider et al., 2014). The GPCC FDM dataset provides monthly precipitation data at a spatial resolution of 0.5° from 1891 to 2020. The GPCC data were sourced from the Deutscher Wetterdienst (German Meteorological Service) website (https://opendata.dwd.de/climate_environment/GPCC/html/fulldata-monthly_v2022_doi_download.html).

The Global Precipitation Climatology Project (GPCP) is a combined satellite-gauge precipitation product overseen by the World Climate Research Program (WCRP) under its Global Water and Energy Experiment (GEWEX) Data and Assessment Panel (GDAP). It integrates rain gauge observations with satellite data to generate global precipitation estimates. For this study, we utilized GPCP v3.2 Satellite-Gauge (SG) Combined Data (Huffman et al., 2023). The monthly GPCP v3.2 dataset spans from 1979 to present at a spatial resolution of 0.5°. The data are available from the Goddard Earth Sciences Data and Information Services Center (https://disc.gsfc.nasa.gov/datasets/GPCPMON_3.2/summary).

2.1.2 TWS from GRACE/GRACE-FO

We analyzed the GRACE/GRACE-FO Level-3 products of the G3P (Güntner et al., 2023) and the JPL Release 6 mascon (Watkins et al., 2015; Wiese et al., 2023) TWS datasets to estimate water storage deficit. TWS comprises the sum of snow, ice, surface water, soil moisture, and groundwater. The G3P TWS data were acquired from the GFZ Information System and

Data Center (ftp://isdcftp.gfz-potsdam.de). The JPL mascon TWS data were downloaded from the Virtual Directories of Earth

130 Data CMR (https://cmr.earthdata.nasa.gov/virtual-directory/collections/C2536962485-POCLOUD/temporal/2002/04/16). Both G3P and JPL mascon offer a higher spatial resolution (0.5°) than do the spherical harmonic solutions and monthly data. However, datasets suffer from missing monthly data, particularly after 2011, due to satellite battery issues. To ensure consistent comparisons between continuous TWS and precipitation time series data, we filled the missing months in the time series by averaging the data from the previous and subsequent two months, resulting in a mean of four months (Andrew et al., 2017;

135 Long et al., 2015). However, there is also a time gap between the GRACE and GRACE-FO missions, spanning from July 2017 (i.e., the end of the science phase of the GRACE mission) to May 2018 (i.e., the launch of GRACE-FO). This period is left missing.

The JPL mascon TWS dataset represents anomalies relative to a long-term mean from January 2004 to December 2009, while

140 the G3P TWS dataset uses a long-term mean from April 2002 to December 2020 as the baseline. To ensure consistent comparisons between the time series, we adjusted the baseline of the JPL mascon TWS to match that of the G3P TWS (Humphrey et al., 2023). This involved averaging each grid point over the period of April 2002 to December 2020 and subtracting it from the entire time series. Thus, this study utilized monthly TWS data from April 2002 to December 2020 for DRT analysis.

145 **2.1.3 Köppen-Geiger Climate Classification**

Globally, the Köppen-Geiger climate classification system, based on temperature and precipitation, is widely used for regional climate zonation by a diverse range of disciplines, such as climate research, physical geography, hydrology, agriculture, biology, and education (Kottek et al., 2006). In response to the need for current and well-documented global climate classifications, a new Köppen-Geiger climate map was released for a high-resolution (0.5°) depiction of global climates for

150 the 1951-2000 period (Kottek et al., 2006). The present study utilized a more recent version of this dataset covering the 1986-2010 period at a higher spatial resolution of 0.083° (Rubel et al., 2017). To achieve consistency with our TWS and precipitation data (grid resolution of 0.5°), the Köppen-Geiger climate classifications were re-gridded using bilinear interpolation. This study focused on the following five main Köppen-Geiger climate categories: equatorial, arid, warm temperate, snow, and polar, as illustrated in Fig. 1. The Köppen-Geiger climate classification scheme used in this study is available at

155 https://koeppen-geiger.vu-wien.ac.at/present.htm.
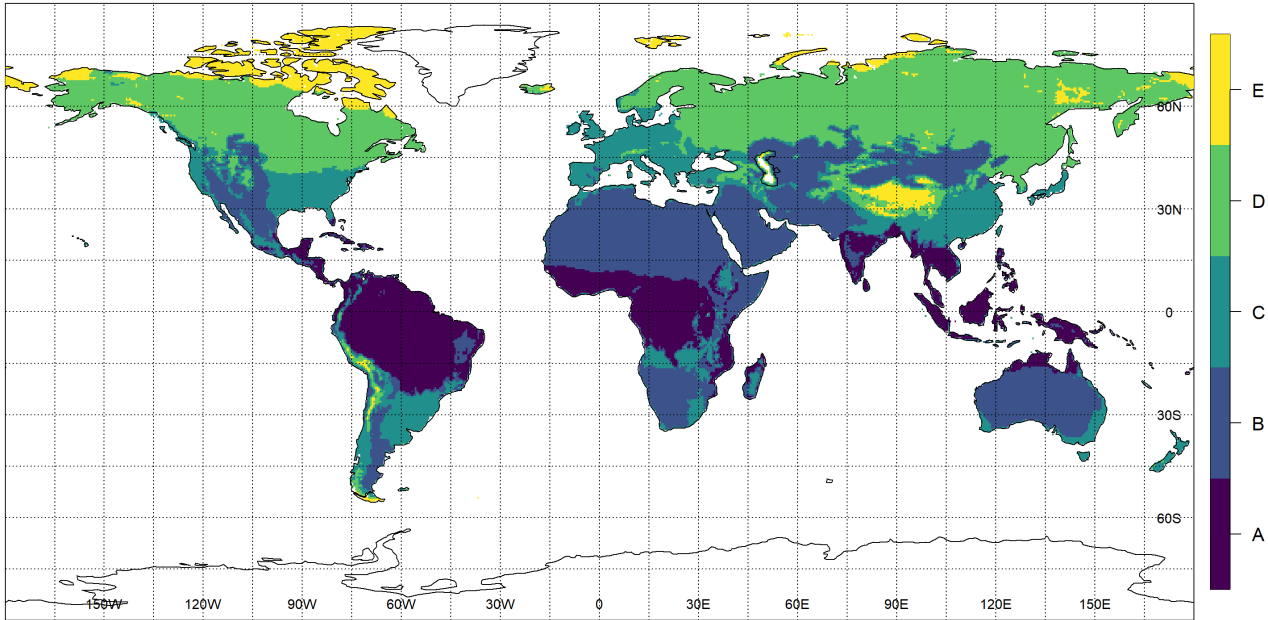
Figure 1. Köppen-Geiger climate zone classification with the five main zones Equatorial (A); Arid (B); Warm Temperatures (C); Snow (D); and Polar (E).

2.2 Water Balance Equation

TWS changes are closely related to precipitation via the water balance equation.

$$ds/dt = P - ET - R \,, \tag{1}$$

where ds/dt is storage change with time, P is precipitation, ET is evapotranspiration, and R is runoff, all usually given in mm equivalent water height per month (mm/month).

Any storage changes with time (ds/dt) must be caused by a water flux, which might be vertically between surface and atmosphere (P or ET). Horizontal fluxes at or underneath the Earth's surface is summarized as lateral runoff (R). Since gravity missions directly observe TWSA relative to a (undefined) long-term mean value, it can be used to derive information about water fluxes at a wide range of timescales. In principle, the difference between two storage estimates separated by 30 days (the usual sampling of the GRACE solutions) allows to derive quantitative information about the amount of precipitation that occurred during this time span.

2.3 Deviation of Storage (dTWSA)

Understanding the magnitude of water deficits remains crucial for determining drought recovery timelines. These water deficits can be directly inferred from the variability in TWSA data (Thomas et al., 2014). First, TWSA is smoothed by a 3-month moving average filter to reduce the high-frequency noise (Singh et al., 2021), resulting in smoothed TWSA (sTWSA).

Variations in water storage can be influenced by long-term factors, such as glacier mass accumulation and/or groundwater extraction. To isolate the impact of such long-term processes, we detrended the TWSA data for each grid by removing the linear trend of relevant grid (Singh et al., 2021). Detrending removes the linear trend, essentially isolating the deviations from this long-term trend, which we referred to as deviations of storage (dTWSA).

$$dTWSA_{x,y,t} = sTWSA_{x,y,t} - trend(sTWSA_{x,y,t}), \tag{2}$$

where $sTWSA_{x,y,t}$ is the smoothed TWSA at x,y grid point and time t, and $trend(sTWSA_{x,y,t})$, is the trend of the smoothed TWSA at x,y grid point and time t.

2.4 Cumulative Detrended Precipitation Anomaly (cdPA)

To ensure consistency with dTWSA, we perform a temporal integration of the precipitation data. Then, cumulative precipitation anomalies (cPA) were obtained by subtracting the mean precipitation observed from April 2002 to December 2020 (reference period) from the actual precipitation data for each product:

$$cPA_{x,y,t} = cP_{x,y,t} - \overline{cP_{x,y}}, \tag{3}$$

where $cP_{x,y,t}$ is cumulated precipitation at x,y grid point and time t, and $\overline{cP_{x,y}}$ is the temporal mean of the cumulative precipitation at x,y grid point.

Similar to dTWSA, we smoothed the cumulative precipitation anomalies (scPA) derived from GPCC and GPCP by applying a 3-month moving average filter (Singh et al., 2021). This process effectively reduced short term fluctuations or noise in the anomaly data. To isolate variations in precipitation anomalies from long-term trends, we further detrended the smoothed precipitation anomalies. This additional step reduced any remaining long-term trends in the precipitation patterns. Finally, the cumulative detrended precipitation anomaly (cdPA) data were obtained.

$$cdPA_{x,y,t} = scPA_{x,y,t} - trend(scPA_{x,y,t}), \tag{4}$$

where $scPA_{x,y,t}$ is the smoothed precipitation anomalies at x,y grid point and time t, and $trend(scPA_{x,y,t})$, is the trend of the smoothed precipitation anomalies at x,y grid point and time t.

2.5 Relationship between dTWSA and cdPA

Variations in the key water fluxes (ET, R, and P) cause fluctuations in TWS, a crucial component of the water budget equation. This study leveraged the assumption of a constant relationship between precipitation and the combined evapotranspiration and runoff (ET+R) flux. This assumption allows us to infer potential variations in precipitation based on changes in TWSA.

This predictive model enables us to estimate the amount of precipitation necessary to balance a water storage deficit. This approach offers a valuable tool for understanding and managing water resources by directly linking precipitation dynamics to

205 changes in TWSA. A linear relationship between dTWSA and cdPA was established to estimate the required precipitation amount as follows:

$$cdPA = \beta_0 + \beta_1 * dTWSA + \varepsilon, \tag{5}$$

where β_0 is the intercept; β_1 is the slope (regression coefficient); and ε represents the residual errors of the fit.

210 The units of cdPA and dTWSA are both in mm/month. Therefore, a β_1 value 1 signifies that cdPA is well represented by dTWSA. In regions where β_1 equals 1, precipitation changes directly translate to storage variations. Conversely, regions with β_1 greater than 1 indicate that some of the local precipitation is immediately transported away and does not change the local storage. This suggests that the variability in storage data only partially captures all precipitation due to other hydrological processes (e.g., ET and R) in these regions. Regions with β_1 less than 1 suggest that a smaller amount of precipitation than 215 needed is sufficient to address the storage deficit. In other words, there must be either additional inflow from other places that is phase-locked with local rain events or severe positive biases in rainfall as seen by GPCC or GPCP, leading to an underestimation of the precipitation required based solely on storage variations (Singh et al., 2021).

Following the study of Singh et al. (2021), we estimated not only regression coefficients (i.e., β_0 and β_1), but also the Pearson's 220 correlation coefficient (ρ) between cdPA and dTWSA as well as maximum drought length over each pixel utilizing 19 years of monthly data (i.e., between 2002 and 2020). We classified the correlation coefficient values as follows: no or insignificant correlation (0.00-0.13), weak correlation (0.14-0.39), moderate correlation (0.40-0.69), and strong correlation (0.70-1.00). Here, a positive relationship is expected between cdPA and dTWSA such that positive (negative) precipitation anomalies should lead to increased (decreased) storage changes. Reverse signs in cdPA and dTWSA anomalies indicate weak or no linear 225 relationship between the two variables. Accordingly, the study of Singh et al. (2021) eliminated the pixels that contain weak or no linear relationship between cdPA and dTWSA (i.e., $\rho < 0$, $\beta_1 < 1$, and maximum drought length < 5 months) from the global analyses. Sampling errors could cause fluctuations around 1, and random variability may cause some of the pixels to have β_1 values slightly less than 1, while these pixels may still have some considerable linear relationship. Accordingly, while the methodology of Singh et al. (2021) masked out regions with $\beta_1 < 1$, in this study, regions with $\beta_1 < 0$ are masked out in 230 addition to regions with $\rho < 0$ and maximum drought length < 5 months.

2.6 DRT

Both TWSA and P will be used to quantify DRT. We closely follow the methodology given by Singh et al. (2021) and utilize two different methods to estimate DRT. The first method, based on storage deficit, utilizes only GRACE data to quantify DRT as the duration of the residuals of TWSA from its climatology. The second method is based on the required precipitation 235 amount derived from both TWSA and precipitation datasets. In this approach, a drought is considered to end when the absolute required precipitation amount surpasses the observed precipitation amount. We will thus utilize two different precipitation products (GPCC and GPCP), two different GRACE storage estimates (G3P and JPL mascon), and two different DRT

estimation methods (storage deficit and required precipitation amount) to study the consequences of those processing choices for different climate zones as defined by the Köppen-Geiger climatology (In total, 8 different DRT will be calculated.).

240 **2.6.1 DRT based on Storage Deficit**

The deviation of TWSA from its climatology can offer valuable insights into drought characteristics. To calculate this deviation, we first create a reference point by averaging TWSA values for each month across the entire time series. For example, to establish the average January TWSA, we would calculate the mean of all January values in the data. This average monthly TWSA represented the climatology for that specific month. Subsequently, we calculated how much each TWSA data
245 point deviated from this average climatology by subtracting the corresponding monthly climatology value. To identify drought events, we first calculated a climatology (long-term average) for TWSA data from both JPL mascon and G3P products using the time series from April 2002 to December 2020. This climatology serves as a reference point for typical TWSA conditions for each month. We then subtracted the corresponding monthly climatology value from each TWSA data point, resulting in residuals. Negative residuals indicate water storage deficits (Thomas et al., 2014). We classified periods with persistent
250 negative residuals lasting longer than three consecutive months as drought events, signifying prolonged periods of below-average water storage (Singh et al., 2021). Negative residuals lasting less than three consecutive months were not classified as droughts. However, if a new negative residual period began within one month of a previous drought recovery, we considered them as a continuation of the same drought event. This approach ensured a cohesive record of drought occurrences over time. By applying these criteria, we were able to establish a comprehensive inventory of drought characteristics for each grid point.
255 This inventory served as the basis for our DRT estimation using the storage deficit method. This method analyzed the duration of negative residuals (i.e., smaller storage values than usual) of dTWSA at each location and time, thereby providing insights into the temporal patterns and the severity of drought events.

2.6.2 DRT based on Required Precipitation Amount

The required precipitation amount is obtained from the linear relationship between dTWSA and cdPA. The storage deficit
260 amount is represented by dTWSA, while cdPA, the output of this relationship, represents the required precipitation amount. To quantify the absolute required precipitation amount, the climatology of precipitation over each pixel was added back into the estimated required precipitation amount. The DRT estimation was then conducted by analyzing the duration during which the observed precipitation amount exceeded the absolute required precipitation amount for any given time and location (Singh et al., 2021). This approach allows for a comprehensive assessment of DRT dynamics across the different regions and periods.

2.7 Accuracy Analysis

2.7.1 Consistency in DRT Estimations

The consistency (level of agreement) between the two DRT estimations was quantified by assessing the differences in the timing obtained from both methods. In this context, consistency referred to the temporal difference between the estimated DRTs from each method, as categorized in Table 1. For example, if the time difference between the two methods fell within 1 or 2 months, the location was categorized as consistency category 1. By comparing the time differences between the DRT estimates from each method for each TWS-precipitation product, we were able to quantify the consistency between the two approaches. This analysis provides valuable insights into the reliability and robustness of the DRT estimations. In essence, it helped us assess how well the two methods converged on similar DRT values for the same locations.

Table 1. Consistency categories in DRT estimations

Consistency category	Time difference (months)
1	1-2
2	3-4
3	5-8
4	9+

2.7.2 Calculated Statistics

In our analyses, we use standard error (SE) as a measure of the uncertainty associated with the means of our datasets. A smaller SE value indicates a more precise estimate of the mean DRT over each pixel, which is often achieved with less variation in the data (Lee et al., 2015). The value of SE was separately calculated for each grid point and climate zone as follows:

$$SE_{x,y} = \frac{SD_{x,y}}{\sqrt{n_{x,y}}},$$ (6)

where $SD_{x,y}$ is the standard deviation of DRT at x,y grid point, and $n_{x,y}$ is the length of the dataset at x,y grid point. In addition to SE, we employed confidence intervals (CIs) to assess the uncertainty around the mean values of our datasets (Curran-Everett, 2008; Lee et al., 2015). CIs provide a range of values that are likely to contain the true population mean with a specified level of confidence (95% in our case) as follows:

$$CI_{x,y} = \mu_{x,y} \mp 1.96 * SE_{x,y},$$ (7)

where $\mu_{x,y}$ is the mean DRT at x,y grid point, and SE is the standard error of DRT at x,y grid point.

3 Results

3.1 Relationship between cdPA and dTWSA

Figure 2a illustrates the spatial distribution of correlation coefficients between dTWSA and cdPA for one selected data combination of dTWSA from G3P and cdPA from GPCP (from now on abbreviated as G3P&GPCP). G3P&GPCP was selected to show actual values since the coupled product has the highest correlation coefficient (0.30). All the correlation coefficient values ≤ 0.13 were not significant ($p > 0.05$; $n = 216$). Significant and moderate correlations were found over Australia (0.55), South America (0.46) and southern Africa (0.60), where not only are water storage variations substantial, but also in situ observing networks are dense. These correlations indicate substantial agreement in these areas. The negative correlations over polar regions (~70% of grids), where water storage decline is strong during and after the melting season without any direct relation to the incoming precipitation, are more than the other regions (~10% of grids). Similar disagreements are found in highly arid climates in Northern Africa and Central Asia, where water storage variations are tiny and GRACE observations are very likely dominated by measurement noise.

In addition, Figures 2b-d show the spatial distribution of differences in these correlation coefficients for the other possible combinations relative to the results obtained for G3P&GPCP. When switching to JPL mascon (Figures 2c), we see differences primarily in arid climates with generally smaller TWS variations and a consequently poor signal-to-noise ratio in the GRACE data, where processing choices (like spatially variable a priori constraints as applied in the mascon) do have a greater effect. GPCC (Fig. 2d, JPL mascon&GPCC) affected correlations to a larger extent than GPCP (Fig. 2c, JPL mascon&GPCP), in particular over places with less dense in situ networks. Given the standard deviation values of correlation differences (Figs. 2c and 2d) due to switching GPCP to GPCC, the variability was higher in Fig. 2d (global average: 0.21) than in Fig. 2c (global average: 0.14). Higher correlations for GPCP confirm the added value of satellite observations in otherwise data-sparse regions (like the Congo catchment in central Africa). However, we also find a number of places where GPCC fits better to GRACE than GPCP which suggests that systematic deficits in satellite observations might also degrade the combined product in certain areas. Despite the differences identified above, we conclude that there is a strong relation between precipitation and storage monitored by satellite gravimetry, implying that GRACE observations should be used more frequently in the future for large-scale hydrometeorological research.
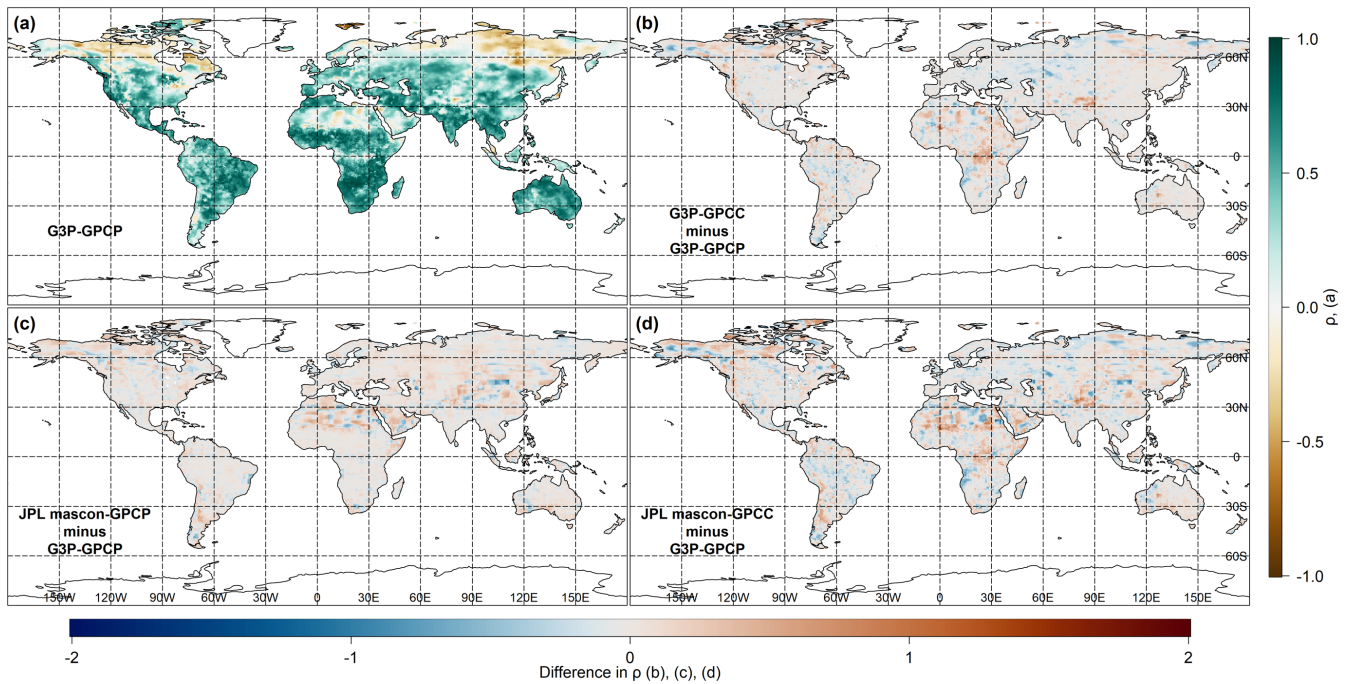
Figure 2. Display of correlation coefficients between different dTWSA (i.e., G3P, JPL mascon) and cdPA (i.e., GPCP, GPCC) datasets. (a) Correlation coefficients obtained for dTWSA from G3P and cdPA from GPCP (G3P&GPCP). Differences in correlation coefficients relative to G3P&GPCP for (b) G3P&GPCC; (c) JPL mascon&GPCP; and (d) JPL mascon&GPCC. Please note that regions with negative correlations were removed from subsequent analyses.

Figure 3a illustrates the spatial distribution of β_1 (Eq. 4), exceeding 0, for G3P&GPCP. We note that certain regions of North Africa, North America, and Northeastern Asia, the β_1 was less than 0. TWS in these regions were likely influenced by factors other than precipitation, thereby making the link between precipitation and TWSA less reliable. Most regions with polar climates (i.e., Köppen-Geiger Climate Zone E) exhibited β_1 below zero, indicating a weak link between precipitation anomalies and changes in TWS in these areas. Similar to the correlation analysis, a contrasting pattern emerged between the arid regions. North America's arid regions (i.e., Zone B) showed a pattern more comparable to Australia's arid regions. Africa's arid regions had a higher percentage of masked-out areas compared to those in Australia and North America. Additionally, the remaining areas in North Africa's arid regions have lower β_1 values.

While switching from G3P to the JPL mascon (Fig. 3c), we note that β_1 values are almost same for the global average (mean difference of Fig. 3c = -0.01). A quite similar pattern is also emerging when switching from GPCP to GPCC (Fig. 3b) and the overall largest decrease in β_1 values are found for the combination G3P&GPCC (-0.06). In particular, using GPCP in Asia's snow zone and Australia's arid zone revealed more regions with β_1 closer to 1 than using GPCC. This suggests less need for additional variables to explain the relationship between precipitation anomalies and TWS changes in these regions when using GPCP than when using GPCC. In Europe's warm temperature zone, the use of the JPL mascon revealed more regions with β_1 larger than 3 compared to that of G3P.
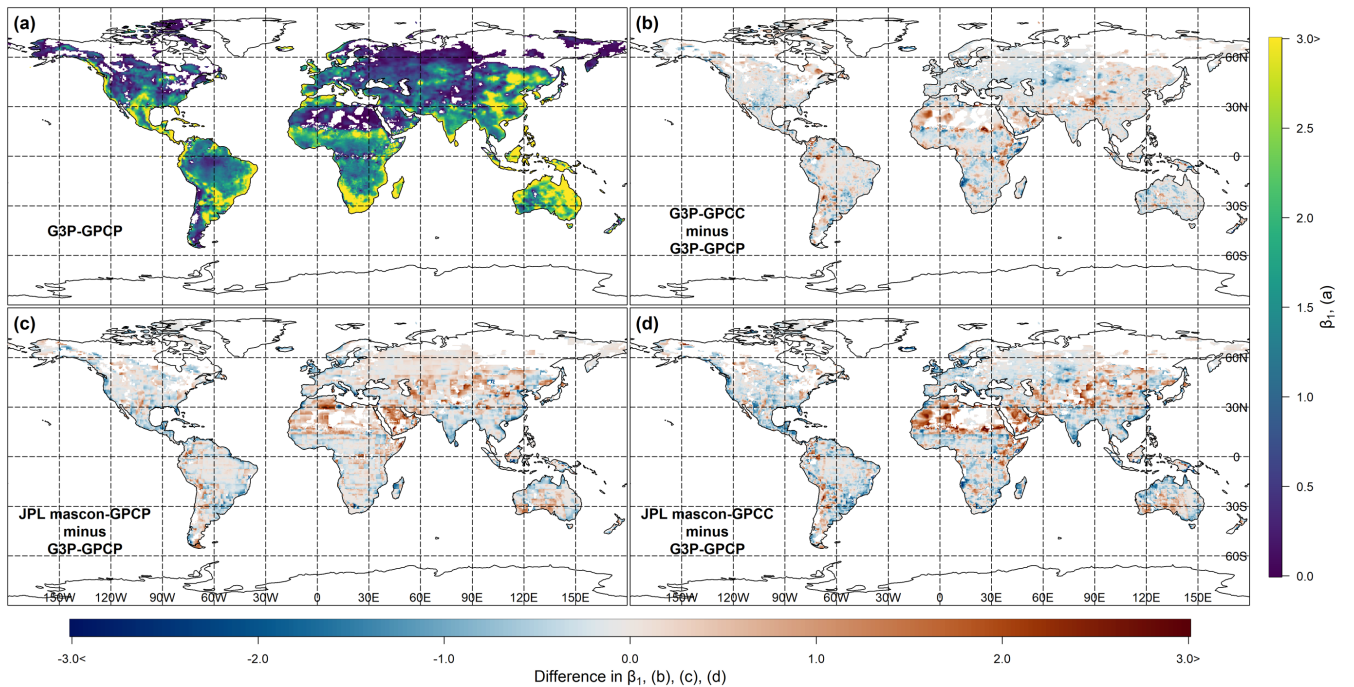
Figure 3. Display of β_1 values between different dTWSA (i.e., G3P, JPL mascon) and cdPA (i.e., GPCP, GPCC) datasets. (a) β_1 values obtained for dTWSA from G3P and cdPA from GPCP (G3P&GPCP). Differences in β_1 values relative to G3P&GPCP for (b) G3P&GPCC, (c) JPL mascon&GPCP, and (d) JPL mascon&GPCC. Regions where β_1 value is smaller than 0 are shown in white. Please note that regions with β_1 value less than 1 were deemed having a weak precipitation-storage relationship and were excluded from subsequent analyses.

Figure 4a displays a time series of dTWSA derived from both G3P and JPL mascon TWSA datasets in an example region in Australia (133.75° E, 16.75° S). Figure 4b illustrates the time series of cdPA derived from both GPCC and GPCP for the same region. These visualizations allow us to observe and analyze the fluctuations in water storage deviations and cdPA over time, providing insights into the dynamics of water availability and precipitation, and potential drought recovery patterns. There existed close agreement between the time series of G3P and JPL mascon, and GPCC and GPCP, as well as between dTWSA and cdPA time series (average ρ = 0.65), as shown in Fig. 4.
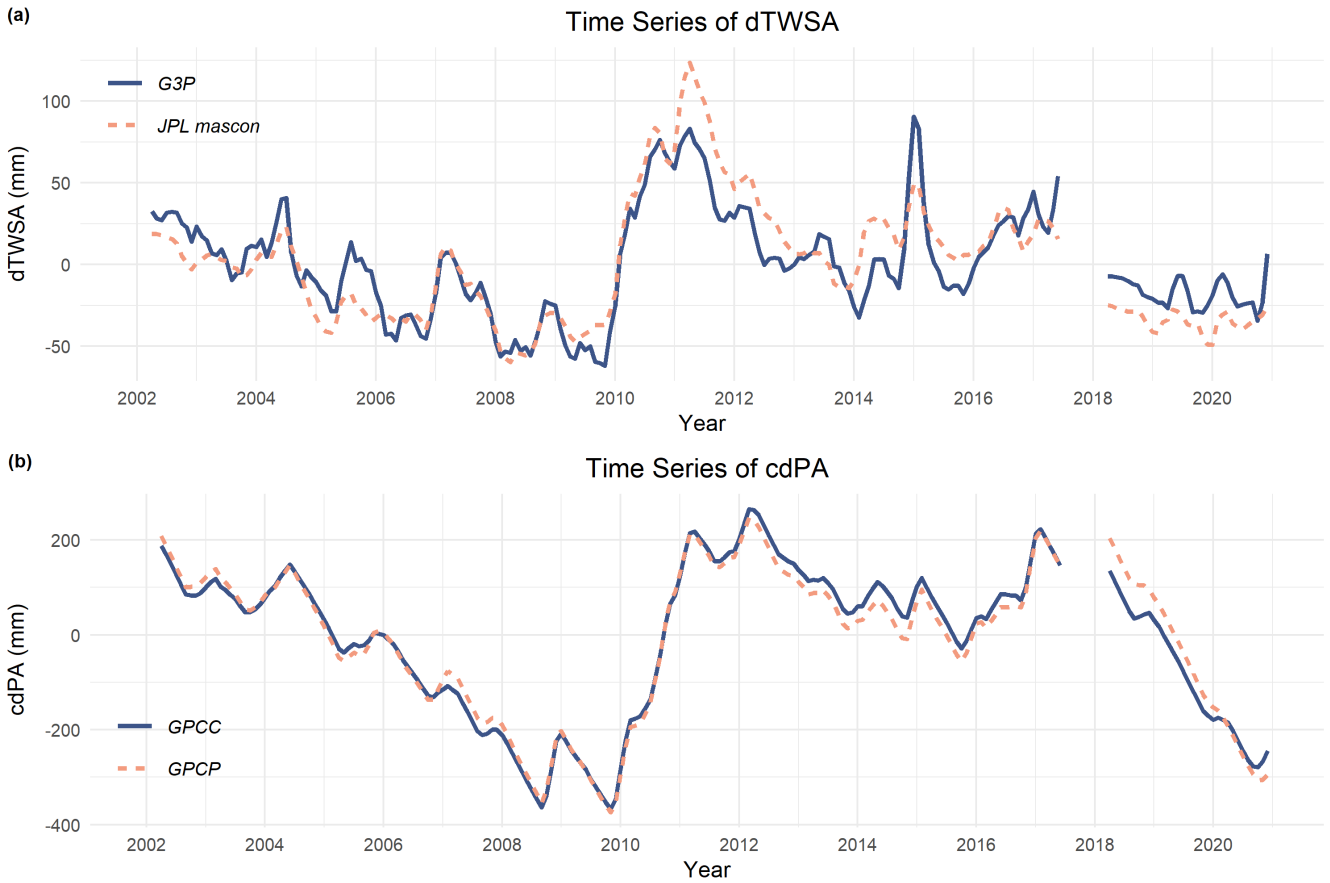
Figure 4. Time series of (a) dTWSA obtained from both G3P and JPL mascon products; and (b) cdPA obtained from both the GPCC and GPCP precipitation products, each in an example region in Australia (133.75° E, 16.75° S).

3.2 DRT Estimations

350 The spatial distributions of mean DRT estimates based on storage deficit and required precipitation amount from the G3P-GPCP coupled product are shown in Figures 5a and 6a, respectively. Figures 5b-d and 6b-d depict the spatial distribution of the differences between the mean DRT estimates derived from G3P&GPCP and G3P&GPCC, JPL mascon&GPCP, and JPL mascon&GPCC, respectively, for both methods. The mean DRT estimations based on storage deficit were identical in Figs. 5a and 5b as well as Figs. 5c and 5d because the DRT estimations relied solely on TWS products for this method. Precipitation

355 products were only used for the exclusion of the regions for this method in Fig. 5. Therefore, the only differences between G3P&GPCP and G3P&GPCC (Fig. 5b) as well as JPL mascon&GPCP (Fig. 5c) and JPL mascon&GPCC (Fig. 5d) were the excluded regions. Even though the required precipitation method incorporated precipitation data into DRT estimations, the overall spatial patterns of mean DRT remained similar between G3P&GPCP and G3P&GPCC (Fig. 6b) as well as JPL mascon&GPCP and JPL mascon&GPCC. Figures 5 and 6 indicated that both the mean and spatial distributions of DRT

360 estimations were consistent with each other using both methods.
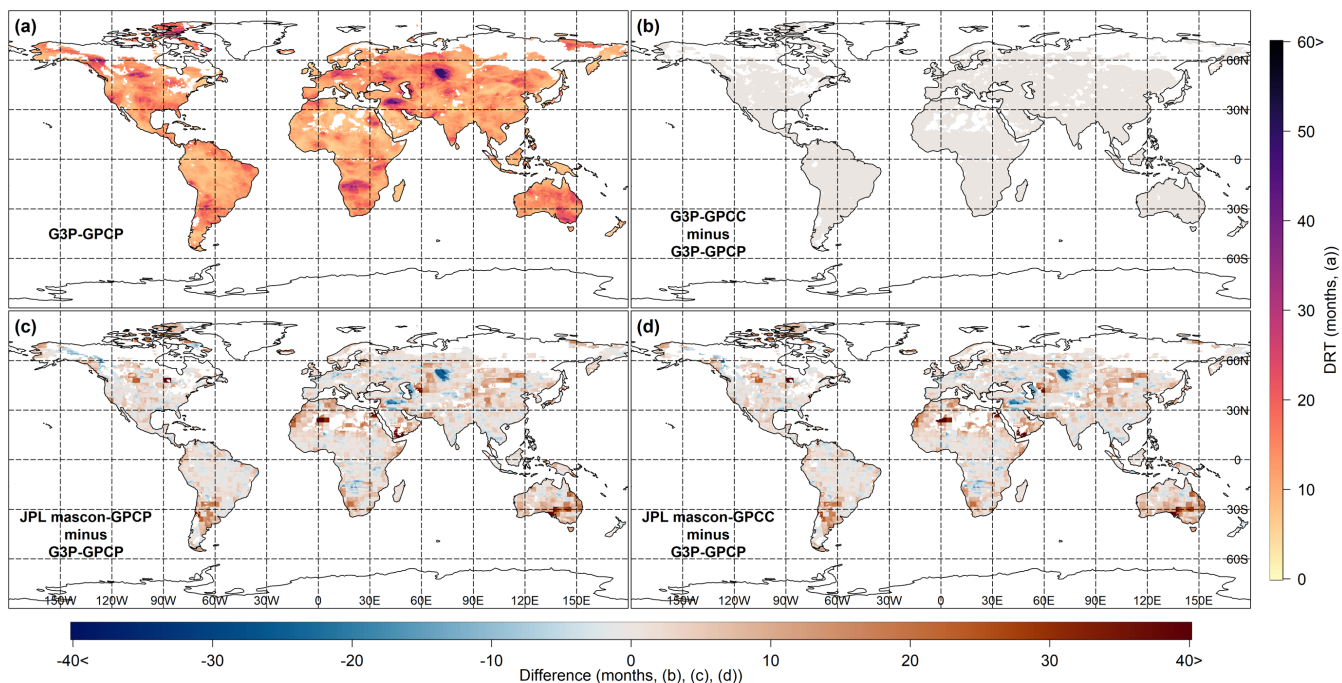
Figure 5. Display of mean drought recovery time (DRT) estimations based on storage deficit obtained from different dTWSA (i.e., G3P, JPL mascon) and cdPA (i.e., GPCP, GPCC) datasets. (a) DRT obtained for dTWSA from G3P and cdPA from GPCP (G3P&GPCP). Differences in DRT relative to G3P&GPCP for (b) G3P&GPCC, (c) JPL mascon&GPCP, and (d) JPL mascon&GPCC.
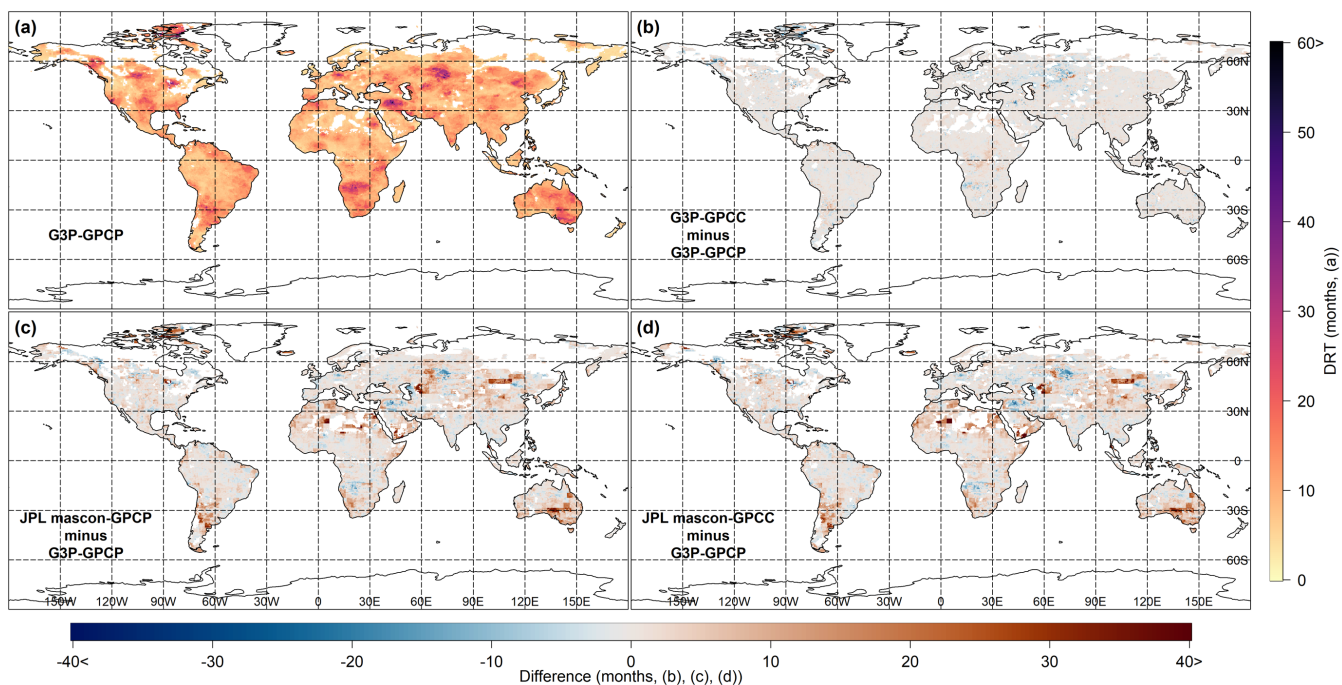
Figure 6. Display of mean drought recovery time (DRT) estimations based on required precipitation obtained from different dTWSA (i.e., G3P, JPL mascon) and cdPA (i.e., GPCP, GPCC) datasets. (a) DRT obtained for dTWSA from G3P and cdPA from GPCP (G3P&GPCP). Differences in DRT relative to G3P&GPCP for (b) G3P&GPCC, (c) JPL mascon&GPCP, and (d) JPL mascon&GPCC.

Figures 5a and 5b, which utilized G3P as TWS product with GPCC and GPCP for precipitation, respectively, reveal the highest mean DRT (50-60 months) estimates based on the storage deficit method in Iran and Central Asia. Likewise, for the required precipitation amount method, Figs. 6a and 6b, which also utilized G3P as TWS product with GPCC and GPCP for precipitation, respectively, showed the highest mean DRT in the same regions. Both methods consistently identified Iran, central Asia, southeastern Australia, and northern Africa as the regions experiencing the highest mean DRT (50-60 months), as illustrated in Figs. 5c and 5d , as well as Figs. 6c and 6d, which utilized JPL mascon as the TWS product with GPCC and GPCP for precipitation, respectively. The spatial correlation between Fig. 5a and 6a is 0.75. This shows a high level of spatial correlation between the Fig. 5a and 6a.

The following other regions exhibited high DRT estimates based on both methods and across all the product combinations: central and southern South America (~40 months), central and southern Africa (~45 months), eastern Australia (~35 months), central and western North America (~40 months), central Europe (~35 months), and eastern Asia (~30 months). Increasing global aridity and drought areas since the mid-20th century mainly as a result of extensive drying in eastern Australia and northern mid-latitude regions, as reported by Dai (2011), are consistent with the findings of high DRT in the present study. Eastern Australia (~35 months) experienced more severe drought conditions than western Australia (~20 months) based on both methods. Consistent with the results of this study, previous research has focused on monitoring droughts in regions with a history of severe, multi-month drought events, such as Iran, central Europe, central and western North America, southeast Australia, and central South America, also, which have experienced higher drought severity compared to other regions (Dai, 2011; Madadgar & Moradkhani, 2014; Rubel et al., 2017; Wu et al., 2023). Over the Colorado River Basin, Madadgar & Moradkhani (2014) observed droughts of varying severity from 2001 to 2004, lasting a total of 48 months, for the period from 2000 to 2011. Our findings for the same region indicate a mean DRT of approximately 30 months. The results of this study (Figs. 5a and 6a) are consistent with those of Boergens et al. (2020), which found that Central Europe is a drought-prone region, experiencing extreme drought during the consecutive summers of 2018 and 2019, with recovery taking over a year. Moreover, the mean DRT estimations obtained from both methods when using JPL mascon were greater than those when using G3P. As shown in Fig. 6, the close agreement between GPCC and GPCP regarding the spatial distribution of mean DRT estimates for both TWS products (G3P and JPL mascon) indicates that the choice of precipitation product (GPCC or GPCP) may not influence the overall spatial patterns of DRT estimates. Figures A1 and A2 illustrate the spatial distributions of the SE of DRT estimates, which were similar to the spatial distributions of the mean DRT estimates. Regions with the highest mean DRT also exhibited the highest SE, indicating that those experiencing longer DRT periods showed greater variability in the DRT estimates.

The mean DRT estimations based on storage deficit and required precipitation amount for the Köppen-Geiger main climate zones using all the TWS-precipitation coupled products are shown in Figs. 7a and 7b, respectively. Error bars representing the 95% confidence intervals for each zone indicate variability in the mean DRT estimates. The "n" values show the number of grids per coupled product within each zone. For both methods, the polar (E) zone exhibited the highest mean DRT (18.1 months for storage deficit, 14.2 months for required precipitation amount). Except the polar (E) zone, consistent with previous findings (Van Lanen et al., 2013), for both methods, the arid (B) zone exhibited the highest mean DRT (14.8 months for storage deficit, 12.9 months for required precipitation amount), while the equatorial (A) zone displayed the lowest (10.9 months for storage deficit, 9.7 months for required precipitation amount). Mean DRT based on storage deficit and required precipitation amount were 13.9 months and 11.4 months in the warm temperature (C) zone, respectively, whereas 14.1 months and 10.0 months in the snow (D) zone, respectively. In particular, all the climate zones except the polar (E) zone displayed minimal variability (< 0.2 months) in the mean DRT (indicated by narrow 95% confidence intervals), suggesting low uncertainty. Overall, the difference between G3P and JPL mascon is the highest in the arid (B, 3.8 months) and polar (E, 5.7 months) zones, whereas the differences in the other zones are smaller than the arid (B) and polar (E) zones. Figures A3a and A3b show SE for the DRT estimations based on storage deficit and required precipitation amount, respectively, across the Köppen-Geiger climate zones for all the TWS-precipitation coupled products. The polar (E) zone had the highest SE for both methods, while the lowest varied by the product. SE for GPCC and GPCP were similar except in the polar (E) zone. JPL mascon estimates had slightly larger SE than G3P for both methods.

(a) *DRT Based on Storage Deficit*

(b) *DRT Based on Required Precipitation Amount*
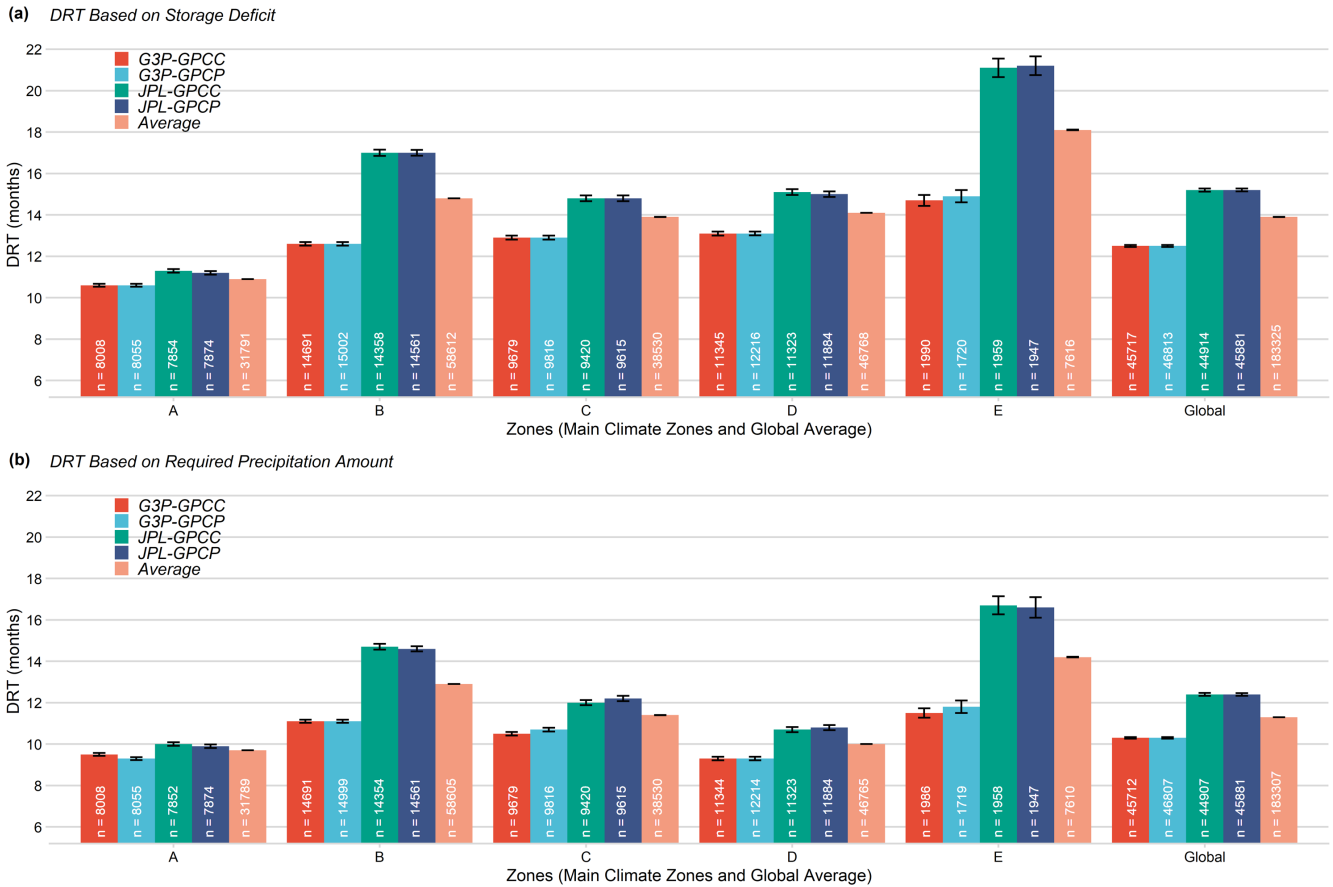
Figure 7. Average DRT estimations based on (a) storage deficit and (b) required precipitation amount for various climate zones from two different dTWSA (i.e., G3P and JPL mascon) and two different cdPA (i.e., GPCP and GPCC) products calculated for Equatorial (A); Arid (B); Warm Temperatures (C); Snow (D); and Polar (E) as given by the Köppen-Geiger classification.

On average, DRT based on storage deficit was estimated as 13.9 months, whereas DRT based on required precipitation amount was estimated as 11.3 months. When considering TWS products, regardless of the precipitation products, DRT estimations using JPL mascon (14.2 months) are consistently higher than DRT estimations using G3P (11.6 months), across all climate zones and the global average. When considering precipitation products, DRT estimations using GPCC and GPCP yielded similar values (12.9 months) regardless of the TWS products across all climate zones and the global average. These findings suggest that GPCC and GPCP closely agree on DRT estimations, and the storage deficit derived from G3P was consistently lower than that from JPL mascon across all zones.

3.3 Consistency in DRT Estimations

Figure 8a shows the spatial distributions of the consistency categories (Table 1) for the DRT estimates from G3P&GPCP coupled products. Figures 8b-d illustrates the spatial distributions of the differences in consistency categories for the DRT estimations between G3P&GPCP and G3P&GPCC, JPL mascon&GPCP, and JPL mascon&GPCC, respectively. Most regions

fell into consistency category 1 (high agreement) and the mean absolute difference between DRT estimations calculated from
435 both methods is 1.9 months. The spatial patterns were similar across all possible data combinations (Figs. 8a-d), including
those using the different TWS (G3P vs. JPL mascon) and precipitation (GPCC vs. GPCP) products. This consistency was also
observed in the mean DRT for all the pairs. As expected, the regions in category 4 (time difference > 9 months) had the highest
mean DRT and SE in both methods (Table 2).

440
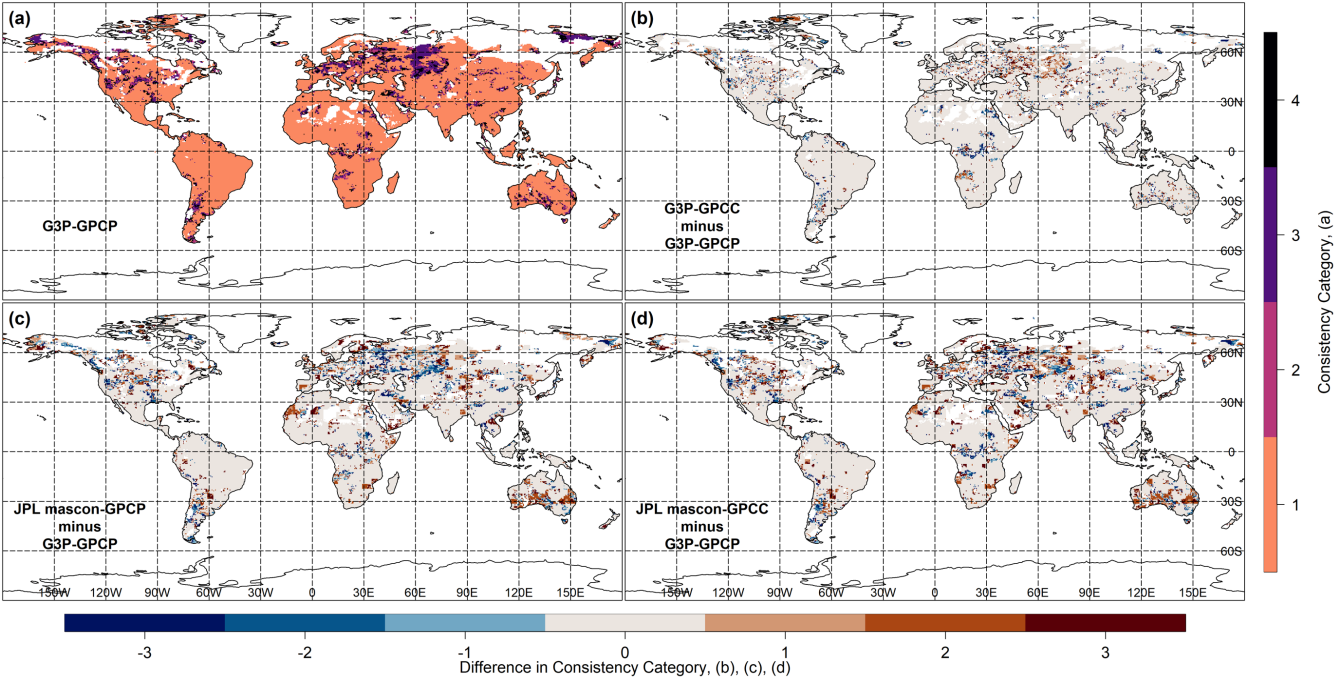
Figure 8. Display of the consistency in DRT estimations based on either storage deficit or required precipitation obtained from different dTWSA (i.e., G3P, JPL mascon) and cdPA (i.e., GPCP, GPCC) datasets. (a) Consistency for dTWSA from G3P and cdPA from GPCP (G3P&GPCP). Differences in consistency relative to G3P&GPCP for (b) G3P&GPCC, (c) JPL mascon&GPCP, and (d) JPL mascon&GPCC.

445 **Table 2. Mean DRT and SE for the Consistency Categories**

	Mean DRT (months)	Mean SE (months)
Category 1	12.2	3.9
Category 2	13.0	4.7
Category 3	16.0	6.9
Category 4	23.1	12.1

Figure 9 shows the consistency levels in terms of the percentage of category 1 (time differences of 1-2 months) for the Köppen-Geiger climate zones using all the coupled products. The polar (E) zone had the lowest average consistency (74.9%), while

the equatorial (A) zone had the highest (97.8%). Overall, 87.5% of DRT estimations achieved category 1 consistency. The consistency rate of G3P (88.5%) is higher than that of JPL mascon (83.5%) across the climate zones and globally. The G3P&GPCP combination achieved the highest consistency (on average, 88.7%), whereas JPL mascon&GPCP and showed the lowest (on average, 82.8%).
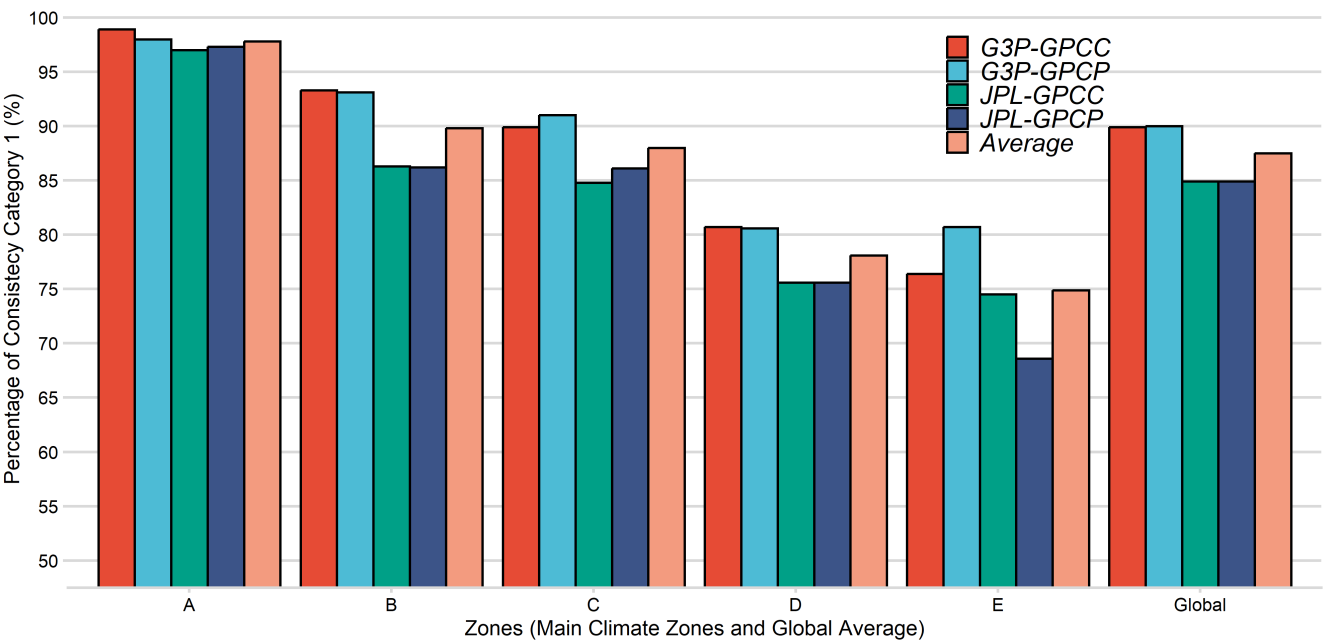
Figure 9. Percentage of DRT estimations whose consistency is category 1 for different climate zones using all the TWS-precipitation coupled products for climates characterized as Equatorial (A); Arid (B); Warm Temperatures (C); Snow (D); and Polar (E) by the Köppen-Geiger classification.

The choice of the precipitation product (GPCC vs. GPCP) exerted minimal impact on consistency (average absolute difference 1.4%) when the same TWS product was used. Conversely, G3P led to higher DRT consistency (average absolute difference 5.0%) than JPL mascon, when the same precipitation product was used. The climate zones also influenced consistency. GPCC and GPCP showed similar consistency in the arid (B, 0.2 months) zone and in the snow (D, 0.1 months) zone and the most different in the polar (E) zone (5.1% difference). In contrast, G3P and JPL mascon had the most similar consistency in the equatorial (A) zone (1.3% difference) and the highest difference in the arid (B) zone and the polar (E) zone (7.0% difference).

3.4 Discussion

Both precipitation products provided similar global mean DRT estimations (12.6 months), with a high consistency rate of 87.5%. The largest discrepancy in mean DRT estimation (0.1 months) was observed in the polar (E) zone, with no significant difference in the snow (D) zone. The consistency between the two precipitation products was less than 1% across all the climate zones.

For the TWS products, the global mean DRT estimation using JPL mascon (13.8 months) was 2.6 months higher than that of G3P (11.4 months). G3P exhibited 5.0% higher global consistency (90.0%) than did JPL mascon (85.0%). The largest difference in mean DRT estimation between G3P (13.2 months) and JPL mascon (18.9 months) occurred in the polar (E) zone, with the smallest difference between G3P (10.0 months) and JPL mascon (10.6 months) in the equatorial (A) zone. The greatest consistency disparity (7.0%) occurred in the polar (E) and arid (B) zones, with G3P (78.6% and 93.3%) outperforming JPL mascon values (71.6% and 86.3%) in the polar and arid zones, respectively. The smallest difference (1.3%) between G3P (98.5%) and JPL mascon (97.2%) was recorded in the equatorial (A) zone. In terms of consistency across all the climate zones, G3P outperformed JPL mascon.

4 Summary and Conclusions

TWS changes from one time epoch to another as observed by satellite gravimetry are closely related to the precipitation amount that occurred during that time interval. The novel observing concept realized with the GRACE and GRACE-FO missions thus provides a unique opportunity to evaluate frequently used global precipitation products timescales of a month and longer. Based on our assessments utilizing TWS (G3P spherical harmonics and JPL mascons) and precipitation (GPCC and GPCP) products, we find a generally high correlation among the two over semi-arid and even wetter climates, some parts of the equatorial, warm temperature and snow zones, with (on global average) the best correspondence between G3P and GPCP. Apart from arid regions with very little storage variability, correlation coefficients are fairly insensitive to the selection of GRACE products. When switching from GPCP to GPCC, however, we identify changes in correlation in particular in Africa and partly also in Central Asia, where in situ station coverage is poor and the impact of satellite-based precipitation information in GPCP is comparatively large due to the sparse coverage with in situ rain gauges that GPCC solely relies on.

GRACE/GRACE-FO directly provides water storage anomalies, offering a novel approach to characterize drought by assessing the storage deficit. The time required for drought recovery can be directly derived from the temporal evolution of these deficits (Singh et al., 2021), enabling the measurement of both drought duration and severity. Both GPCC and GPCP products exhibited not only similar DRT estimations but also comparable consistency in their DRT estimations globally and across all the Köppen-Geiger climate zones. For TWS products, the mean DRT estimations from JPL mascon were, on average, 2.6 months higher than those from G3P, globally and across all the Köppen-Geiger climate zones. However, G3P showed slightly higher consistency in the DRT estimations (5.0% difference, globally) than did JPL mascon. Furthermore, G3P demonstrated greater consistency than JPL mascon across all the Köppen-Geiger climate zones.

The results of our study underline the potential value of GRACE for hydrometeorologic research due to the tight relationship between precipitation and TWS changes. Its global coverage (with albeit rather low spatial resolution) allows the testing of different precipitation products not only from combinations of varying satellite and in situ observations (as performed in this

500 study) but also from numerical weather prediction models and global atmospheric reanalyses. Both NASA and also the European Space Agency (ESA) are currently working on future satellite gravity missions with even more precise sensors, so that further improvements in the quality of satellite gravimetry products for hydrologic applications can be expected.

Appendix A

Table A1. The full forms glossary for the abbreviations

cdPA	Cumulative Detrended Precipitation Anomaly
cPA	Cumulative Precipitation Anomaly
DRT	Drought Recovery Time
dTWSA	Deviation of Storage
G3P	Global Gravity-based Groundwater Project
GPCC	Global Precipitation Climatology Center
GPCC FDM	Global Precipitation Climatology Center Full Data Monthly Product
GPCP	Global Precipitation Climatology Project
JPL mascons	Jet Propulsion Laboratory Mass Concentration blocks
scPA	Smoothed Cumulative Precipitation Anomaly
TWS	Terrestrial Water Storage
TWSA	Terrestrial Water Storage Anomaly

505
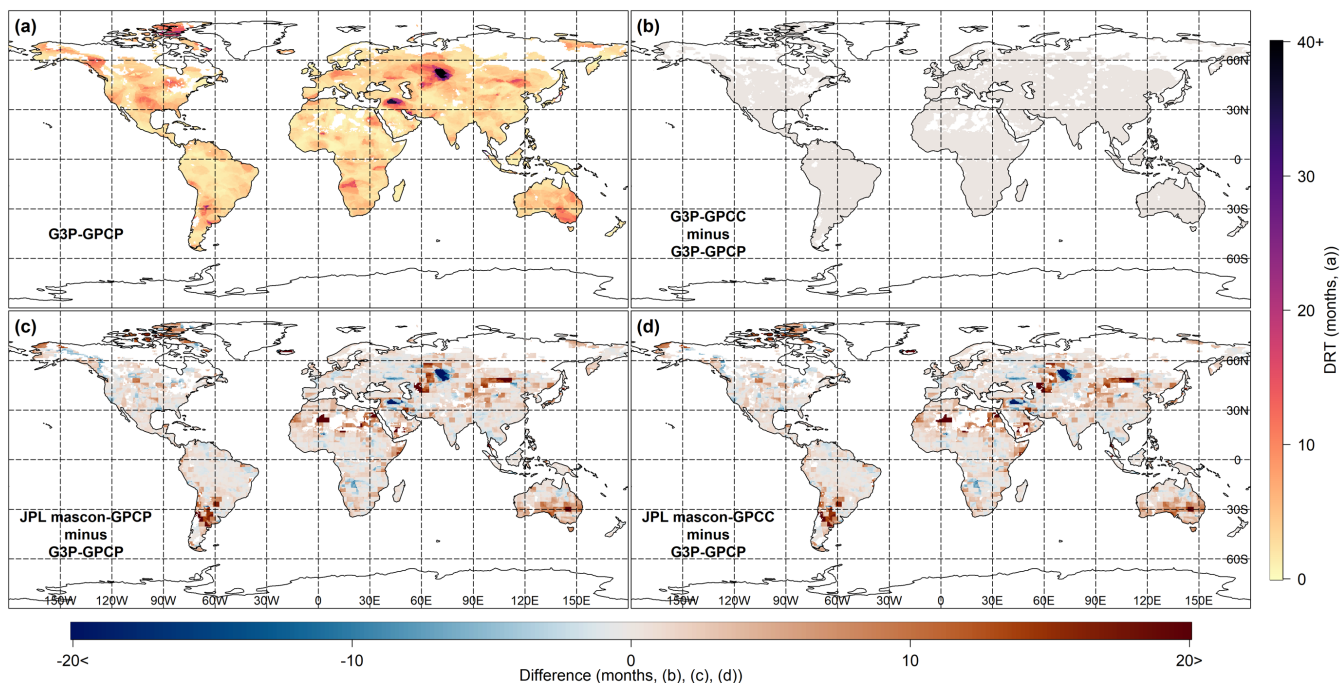
Figure A1. Display of the standard error of DRT estimations based on the storage deficit obtained from different dTWSA (i.e., G3P, JPL mascon) and cdPA (i.e., GPCP, GPCC) datasets. (a) Standard error for dTWSA from G3P and cdPA from GPCP (G3P&GPCP). Differences in standard error relative to G3P&GPCP for (b) G3P&GPCC, (c) JPL mascon&GPCP, and (d) JPL mascon&GPCC.

510
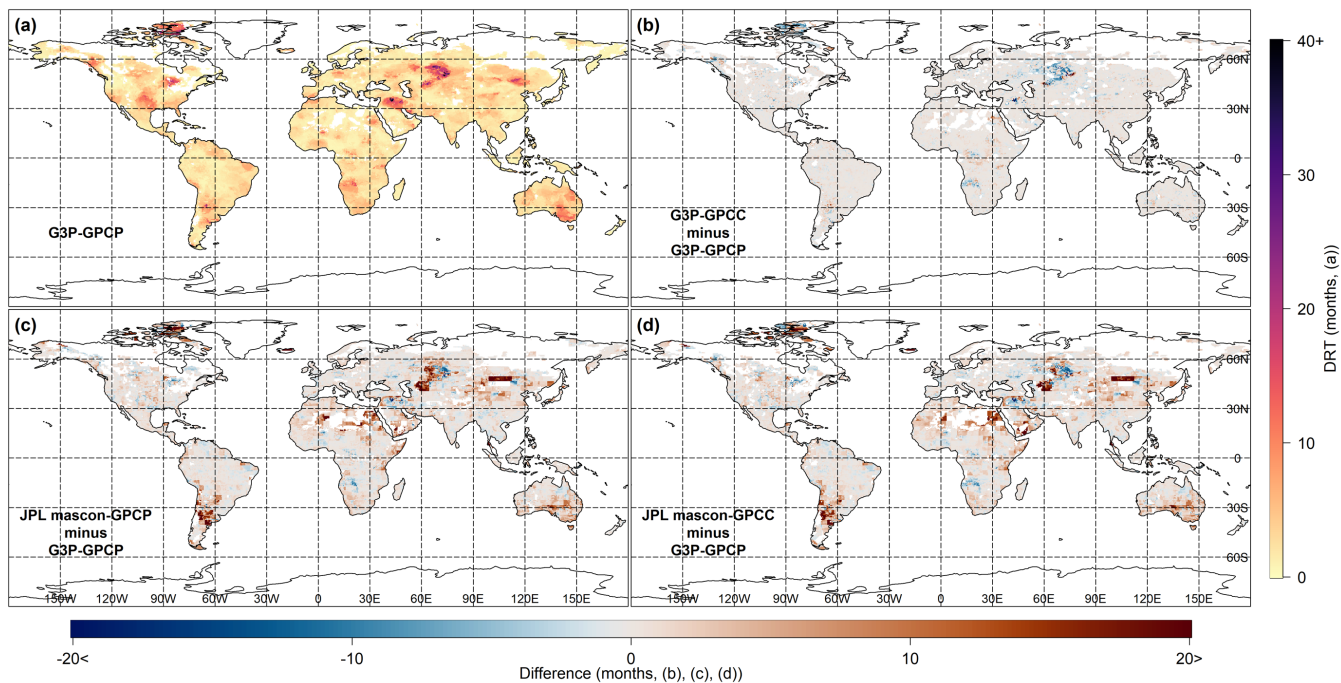
Figure A2. Display of the standard error of DRT estimations based on the required precipitation obtained from different dTWSA (i.e., G3P, JPL mascon) and cdPA (i.e., GPCP, GPCC) datasets. (a) Standard error for dTWSA from G3P and cdPA from GPCP (G3P&GPCP). Differences in standard error relative to G3P&GPCP for (b) G3P&GPCC, (c) JPL mascon&GPCP, and (d) JPL mascon&GPCC.
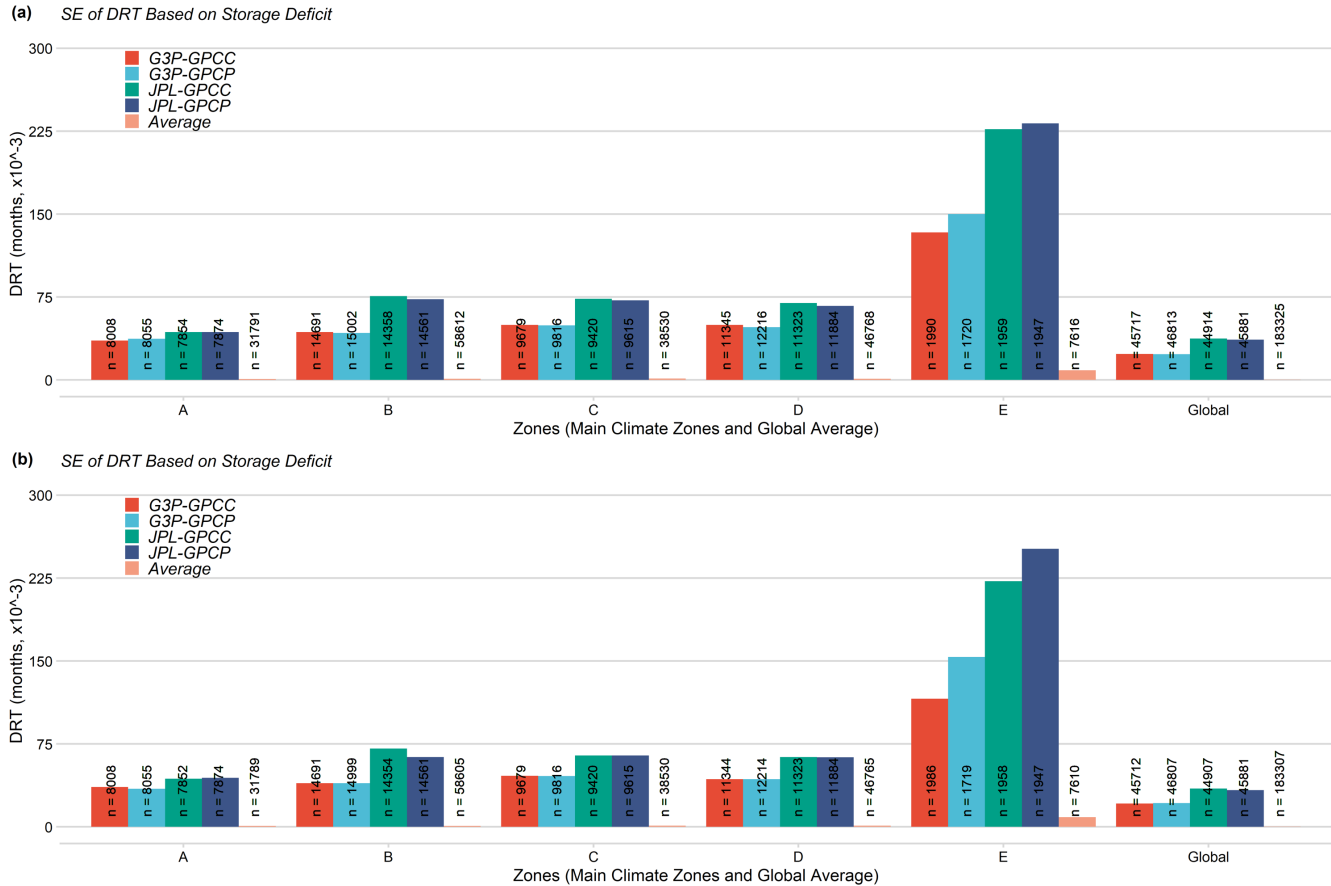
Figure A3. Standard error for average DRT estimations based on (a) storage deficit and (b) required precipitation amount for various climate zones from two different dTWSA (i.e., G3P and JPL mascon) and two different cdPA (i.e., GPCP and GPCC) products calculated for Equatorial (A); Arid (B); Warm Temperatures (C); Snow (D); and Polar (E) as given by the Köppen-Geiger classification.

Data Availability

The datasets used for this study are publicly available under the following links. JPL mascon GRACE and GRACE-FO TWS: https://cmr.earthdata.nasa.gov/virtual-directory/collections/C2536962485-POCLOUD/temporal/2002/04/16; G3P GRACE and GRACE-FO TWS: ftp://isdcftp.gfz-potsdam.de; GPCC Full Data Monthly precipitation: https://opendata.dwd.de/climate_environment/GPCC/html/fulldata-monthly_v2022_doi_download.html; GPCP v3.2 Satellite-Gauge (SG) Combined Data: https://disc.gsfc.nasa.gov/datasets/GPCPMON_3.2/summary; Köppen-Geiger climate classification scheme: https://koeppen-geiger.vu-wien.ac.at/present.htm.

Author Contribution

ÇÇ contributed to conceptualization, data curation, formal analysis, investigation, methodology, resources, software, validation, visualization, preparing the original draft, and editing the manuscript according to the reviews from the co-authors. MTY contributed to funding acquisition, project administration, supervision, resources, and reviewing and editing the manuscript. HD contributed to conceptualization, methodology, supervision, and reviewing and editing the manuscript. ESI contributed to funding acquisition, project administration, supervision, and reviewing and editing the manuscript. FE, CF, and ALY contributed to funding acquisition, and reviewing and editing the manuscript.

Competing Interests

The authors declare that they have no conflict of interest.

Acknowledgments

We thank the German Research Center for Geosciences (GFZ) and Jet Propulsion Laboratory (JPL) for providing GRACE and GRACE-FO datasets; Deutscher Wetterdienst (DWD) for providing the GPCC Full Data Monthly Product; Goddard Earth Sciences Data and Information Services Center (GES DISC) for providing GPCP version 3.2 Satellite-Gauge Combined Precipitation dataset; The University of Veterinary Medicine, Vienna for providing Updated World Map of the Köppen-Geiger Climate Classification. This study is funded by The Scientific and Technological Research Council of Turkey (TUBITAK) Grant Number 120R065 and the Federal Ministry of Education and Research (BMBF) with the Grant Number 01DL22002.

References

Adler, R. F., Huffman, G. J., Chang, A., Ferraro, R., Xie, P.-P., Janowiak, J., Rudolf, B., Schneider, U., Curtis, S., Bolvin, D., Gruber, A., Susskind, J., Arkin, P., & Nelkin, E. (2003). The Version-2 Global Precipitation Climatology Project (GPCP) Monthly Precipitation Analysis (1979–Present). *Journal of Hydrometeorology*, *4*(6), 1147–1167. https://doi.org/10.1175/1525-7541(2003)004<1147:TVGPCP>2.0.CO;2

AghaKouchak, A., Farahmand, A., Melton, F. S., Teixeira, J., Anderson, M. C., Wardlow, B. D., & Hain, C. R. (2015). Remote sensing of drought: Progress, challenges and opportunities. *Reviews of Geophysics*, *53*(2), 452–480. https://doi.org/10.1002/2014RG000456

Akbari Asanjan, A., Yang, T., Hsu, K., Sorooshian, S., Lin, J., & Peng, Q. (2018). Short-Term Precipitation Forecast Based on the PERSIANN System and LSTM Recurrent Neural Networks. *Journal of Geophysical Research: Atmospheres*, *123*(22). https://doi.org/10.1029/2018JD028375

555 Ali, A., Amani, A., Diedhiou, A., & Lebel, T. (2005). Rainfall Estimation in the Sahel. Part II: Evaluation of Rain Gauge Networks in the CILSS Countries and Objective Intercomparison of Rainfall Products. *Journal of Applied Meteorology*, *44*(11), 1707–1722. https://doi.org/10.1175/JAM2305.1

Andrew, R. L., Guan, H., & Batelaan, O. (2017). Large-scale vegetation responses to terrestrial moisture storage changes. *Hydrology and Earth System Sciences*, *21*(9), 4469–4478. https://doi.org/10.5194/hess-21-4469-2017

560 Bai, X., Wu, X., & Wang, P. (2019). Blending long-term satellite-based precipitation data with gauge observations for drought monitoring: Considering effects of different gauge densities. *Journal of Hydrology*, *577*, 124007. https://doi.org/10.1016/j.jhydrol.2019.124007

Barker, L. J., Hannaford, J., Chiverton, A., & Svensson, C. (2016). From meteorological to hydrological drought using standardised indicators. *Hydrology and Earth System Sciences*, *20*(6), 2483–2505. https://doi.org/10.5194/hess-20-
565   2483-2016

Bayar, A. S., Yılmaz, M. T., Yücel, İ., & Dirmeyer, P. (2023). CMIP6 Earth System Models Project Greater Acceleration of Climate Zone Change Due To Stronger Warming Rates. *Earth's Future*, *11*(4), e2022EF002972. https://doi.org/10.1029/2022EF002972

Beck, H. E., Vergopolan, N., Pan, M., Levizzani, V., Van Dijk, A. I. J. M., Weedon, G. P., Brocca, L., Pappenberger, F.,
570   Huffman, G. J., & Wood, E. F. (2017). Global-scale evaluation of 22 precipitation datasets using gauge observations and hydrological modeling. *Hydrology and Earth System Sciences*, *21*(12), 6201–6217. https://doi.org/10.5194/hess-21-6201-2017

Behrangi, A., Nguyen, H., & Granger, S. (2015). Probabilistic Seasonal Prediction of Meteorological Drought Using the Bootstrap and Multivariate Information. *Journal of Applied Meteorology and Climatology*, *54*(7), 1510–1522.
575   https://doi.org/10.1175/JAMC-D-14-0162.1

Belabid, N., Zhao, F., Brocca, L., Huang, Y., & Tan, Y. (2019). Near-Real-Time Flood Forecasting Based on Satellite Precipitation Products. *Remote Sensing*, *11*(3), 252. https://doi.org/10.3390/rs11030252

Boergens, E., Güntner, A., Dobslaw, H., & Dahle, C. (2020). Quantifying the Central European Droughts in 2018 and 2019 With GRACE Follow-On. *Geophysical Research Letters*, *47*(14), e2020GL087285. https://doi.org/10.1029/2020GL087285

Curran-Everett, D. (2008). Explorations in statistics: Standard deviations and standard errors. *Advances in Physiology Education*, *32*(3), 203–208. https://doi.org/10.1152/advan.90123.2008

Dai, A. (2011). Drought under global warming: A review. *WIREs Climate Change*, *2*(1), 45–65. https://doi.org/10.1002/wcc.81

Darand, M., & Khandu, K. (2020). Statistical evaluation of gridded precipitation datasets using rain gauge observations over Iran. *Journal of Arid Environments*, *178*, 104172. https://doi.org/10.1016/j.jaridenv.2020.104172

Ding, Y., Xu, J., Wang, X., Peng, X., & Cai, H. (2020). Spatial and temporal effects of drought on Chinese vegetation under different coverage levels. *Science of The Total Environment*, *716*, 137166. https://doi.org/10.1016/j.scitotenv.2020.137166

Döll, P., Hasan, H. M. M., Schulze, K., Gerdener, H., Börger, L., Shadkam, S., Ackermann, S., Hosseini-Moghari, S.-M., Müller Schmied, H., Güntner, A., & Kusche, J. (2024). Leveraging multi-variable observations to reduce and quantify the output uncertainty of a global hydrological model: Evaluation of three ensemble-based approaches for the Mississippi River basin. *Hydrology and Earth System Sciences*, *28*(10), 2259–2295. https://doi.org/10.5194/hess-28-2259-2024

Eicker, A., Schumacher, M., Kusche, J., Döll, P., & Schmied, H. M. (2014). Calibration/Data Assimilation Approach for Integrating GRACE Data into the WaterGAP Global Hydrology Model (WGHM) Using an Ensemble Kalman Filter: First Results. *Surveys in Geophysics*, *35*(6), 1285–1309. https://doi.org/10.1007/s10712-014-9309-8

Gebrechorkos, S. H., Leyland, J., Dadson, S. J., Cohen, S., Slater, L., Wortmann, M., Ashworth, P. J., Bennett, G. L., Boothroyd, R., Cloke, H., Delorme, P., Griffith, H., Hardy, R., Hawker, L., McLelland, S., Neal, J., Nicholas, A., Tatem, A. J., Vahidi, E., … Darby, S. E. (2024). Global-scale evaluation of precipitation datasets for hydrological modelling. *Hydrology and Earth System Sciences*, *28*(14), 3099–3118. https://doi.org/10.5194/hess-28-3099-2024

Golian, S., Javadian, M., & Behrangi, A. (2019). On the use of satellite, gauge, and reanalysis precipitation products for drought studies. *Environmental Research Letters*, *14*(7), 075005. https://doi.org/10.1088/1748-9326/ab2203

Güntner, A., Sharifi, E., Behzadpour, S., Boergens, E., Dahle, C., Darbeheshti, N., Dobslaw, H., Dorigo, W., Dussailant, I., Flechtner, F., Haas, J., Jäggi, A., Kidd, R., Kosmale, M., Kvas, A., Luojus, K., Mayer-Gürr, T., Meyer, U., Pasik, A., … Zemp, M. (2023). *Global Gravity-based Groundwater Product (G3P)* (Version 1.11) [Dataset]. GFZ Data Services. https://doi.org/10.5880/G3P.2023.001

Harris, A., Rahman, S., Hossain, F., Yarborough, L., Bagtzoglou, A. C., & Easson, G. (2007). Satellite-based Flood Modeling Using TRMM-based Rainfall Products. *Sensors*, *7*(12), 3416–3427. https://doi.org/10.3390/s7123416

Huffman, G. J., Adler, R. F., Behrangi, A., Bolvin, D. T., Nelkin, E. J., Gu, G., & Ehsani, M. R. (2023). The New Version 3.2 Global Precipitation Climatology Project (GPCP) Monthly and Daily Precipitation Products. *Journal of Climate*, *36*(21), 7635–7655. https://doi.org/10.1175/JCLI-D-23-0123.1

Humphrey, V., Rodell, M., & Eicker, A. (2023). Using Satellite-Based Terrestrial Water Storage Data: A Review. *Surveys in Geophysics*, *44*(5), 1489–1517. https://doi.org/10.1007/s10712-022-09754-9

Keyantash, J., & Dracup, J. A. (2002). The Quantification of Drought: An Evaluation of Drought Indices. *Bulletin of the American Meteorological Society*, *83*(8), 1167–1180. https://doi.org/10.1175/1520-0477-83.8.1167

Kottek, M., Grieser, J., Beck, C., Rudolf, B., & Rubel, F. (2006). World Map of the Köppen-Geiger climate classification updated. *Meteorologische Zeitschrift*, *15*(3), 259–263. https://doi.org/10.1127/0941-2948/2006/0130

Lai, C., Li, J., Wang, Z., Wu, X., Zeng, Z., Chen, X., Lian, Y., Yu, H., Wang, P., & Bai, X. (2018). Drought-Induced Reduction in Net Primary Productivity across Mainland China from 1982 to 2015. *Remote Sensing*, *10*(9), 1433. https://doi.org/10.3390/rs10091433

Lai, C., Zhong, R., Wang, Z., Wu, X., Chen, X., Wang, P., & Lian, Y. (2019). Monitoring hydrological drought using long-term satellite-based precipitation data. *Science of The Total Environment*, *649*, 1198–1208. https://doi.org/10.1016/j.scitotenv.2018.08.245

Lamptey, B. L. (2008). Comparison of Gridded Multisatellite Rainfall Estimates with Gridded Gauge Rainfall over West Africa. *Journal of Applied Meteorology and Climatology*, *47*(1), 185–205. https://doi.org/10.1175/2007JAMC1586.1

Lee, D. K., In, J., & Lee, S. (2015). Standard deviation and standard error of the mean. *Korean Journal of Anesthesiology*, *68*(3), 220. https://doi.org/10.4097/kjae.2015.68.3.220

Long, D., Yang, Y., Wada, Y., Hong, Y., Liang, W., Chen, Y., Yong, B., Hou, A., Wei, J., & Chen, L. (2015). Deriving scaling factors using a global hydrological model to restore GRACE total water storage changes for China's Yangtze River Basin. *Remote Sensing of Environment*, *168*, 177–193. https://doi.org/10.1016/j.rse.2015.07.003

Madadgar, S., & Moradkhani, H. (2014). Spatio-temporal drought forecasting within Bayesian networks. *Journal of Hydrology*, *512*, 134–146. https://doi.org/10.1016/j.jhydrol.2014.02.039

Maggioni, V., & Massari, C. (2018). On the performance of satellite precipitation products in riverine flood modeling: A review. *Journal of Hydrology*, *558*, 214–224. https://doi.org/10.1016/j.jhydrol.2018.01.039

Mishra, A. K., & Singh, V. P. (2010). A review of drought concepts. *Journal of Hydrology*, *391*(1–2), 202–216. https://doi.org/10.1016/j.jhydrol.2010.07.012

Negrón Juárez, R. I., Li, W., Fu, R., Fernandes, K., & De Oliveira Cardoso, A. (2009). Comparison of Precipitation Datasets over the Tropical South American and African Continents. *Journal of Hydrometeorology*, *10*(1), 289–299. https://doi.org/10.1175/2008JHM1023.1

Patz, J. A., Frumkin, H., Holloway, T., Vimont, D. J., & Haines, A. (2014). Climate Change: Challenges and Opportunities for Global Health. *JAMA*, *312*(15), 1565. https://doi.org/10.1001/jama.2014.13186

Pfeffer, J., Cazenave, A., Blazquez, A., Decharme, B., Munier, S., & Barnoud, A. (2023). Assessment of pluri-annual and decadal changes in terrestrial water storage predicted by global hydrological models in comparison with the GRACE satellite gravity mission. *Hydrology and Earth System Sciences*, *27*(20), 3743–3768. https://doi.org/10.5194/hess-27-3743-2023

Piao, S., Ciais, P., Huang, Y., Shen, Z., Peng, S., Li, J., Zhou, L., Liu, H., Ma, Y., Ding, Y., Friedlingstein, P., Liu, C., Tan, K., Yu, Y., Zhang, T., & Fang, J. (2010). The impacts of climate change on water resources and agriculture in China. *Nature*, *467*(7311), 43–51. https://doi.org/10.1038/nature09364

Prakash, S., Gairola, R. M., & Mitra, A. K. (2015). Comparison of large-scale global land precipitation from multisatellite and reanalysis products with gauge-based GPCC data sets. *Theoretical and Applied Climatology*, *121*(1–2), 303–317. https://doi.org/10.1007/s00704-014-1245-5

Rubel, F., Brugger, K., Haslinger, K., & Auer, I. (2017). The climate of the European Alps: Shift of very high resolution Köppen-Geiger climate zones 1800–2100. *Meteorologische Zeitschrift*, *26*(2), 115–125. https://doi.org/10.1127/metz/2016/0816

Schneider, U., Becker, A., Finger, P., Meyer-Christoffer, A., Ziese, M., & Rudolf, B. (2014). GPCC's new land surface precipitation climatology based on quality-controlled in situ data and its role in quantifying the global water cycle. *Theoretical and Applied Climatology*, *115*(1–2), 15–40. https://doi.org/10.1007/s00704-013-0860-x

Senocak, A. U. G., Yilmaz, M. T., Kalkan, S., Yucel, I., & Amjad, M. (2023). An explainable two-stage machine learning approach for precipitation forecast. *Journal of Hydrology*, *627*, 130375. https://doi.org/10.1016/j.jhydrol.2023.130375

Shukla, S., & Wood, A. W. (2008). Use of a standardized runoff index for characterizing hydrologic drought. *Geophysical Research Letters*, *35*(2), 2007GL032487. https://doi.org/10.1029/2007GL032487

Singh, A., Reager, J. T., & Behrangi, A. (2021). Estimation of hydrological drought recovery based on precipitation and Gravity Recovery and Climate Experiment (GRACE) water storage deficit. *Hydrology and Earth System Sciences*, *25*(2), 511–526. https://doi.org/10.5194/hess-25-511-2021

Springer, A., Eicker, A., Bettge, A., Kusche, J., & Hense, A. (2017). Evaluation of the Water Cycle in the European COSMO-REA6 Reanalysis Using GRACE. *Water*, *9*(4), 289. https://doi.org/10.3390/w9040289

Sun, Q., Miao, C., Duan, Q., Ashouri, H., Sorooshian, S., & Hsu, K. (2018). A Review of Global Precipitation Data Sets: Data Sources, Estimation, and Intercomparisons. *Reviews of Geophysics*, *56*(1), 79–107. https://doi.org/10.1002/2017RG000574

Tangdamrongsub, N., Jasinski, M. F., & Shellito, P. J. (2021). Development and evaluation of 0.05° terrestrial water storage estimates using Community Atmosphere Biosphere Land Exchange (CABLE) land surface model and assimilation

of GRACE data. *Hydrology and Earth System Sciences*, *25*(7), 4185–4208. https://doi.org/10.5194/hess-25-4185-2021

675 Thomas, A. C., Reager, J. T., Famiglietti, J. S., & Rodell, M. (2014). A GRACE-based water storage deficit approach for hydrological drought characterization. *Geophysical Research Letters*, *41*(5), 1537–1545. https://doi.org/10.1002/2014GL059323

Van Lanen, H. A. J., Wanders, N., Tallaksen, L. M., & Van Loon, A. F. (2013). Hydrological drought across the world: Impact of climate and physical catchment structure. *Hydrology and Earth System Sciences*, *17*(5), 1715–1732.
680 https://doi.org/10.5194/hess-17-1715-2013

Vicente-Serrano, S. M., Beguería, S., López-Moreno, J. I., Angulo, M., & El Kenawy, A. (2010). A New Global 0.5° Gridded Dataset (1901–2006) of a Multiscalar Drought Index: Comparison with Current Drought Index Datasets Based on the Palmer Drought Severity Index. *Journal of Hydrometeorology*, *11*(4), 1033–1043. https://doi.org/10.1175/2010JHM1224.1

685 Vicente-Serrano, S. M., López-Moreno, J. I., Beguería, S., Lorenzo-Lacruz, J., Azorin-Molina, C., & Morán-Tejeda, E. (2012). Accurate Computation of a Streamflow Drought Index. *Journal of Hydrologic Engineering*, *17*(2), 318–332. https://doi.org/10.1061/(ASCE)HE.1943-5584.0000433

Wahr, J., Swenson, S., Zlotnicki, V., & Velicogna, I. (2004). Time-variable gravity from GRACE: First results. *Geophysical Research Letters*, *31*(11), 2004GL019779. https://doi.org/10.1029/2004GL019779

690 Wang, Z., Zhong, R., & Lai, C. (2017). Evaluation and hydrologic validation of TMPA satellite precipitation product downstream of the Pearl River Basin, China. *Hydrological Processes*, *31*(23), 4169–4182. https://doi.org/10.1002/hyp.11350

Watkins, M. M., Wiese, D. N., Yuan, D., Boening, C., & Landerer, F. W. (2015). Improved methods for observing Earth's time variable mass distribution with GRACE using spherical cap mascons. *Journal of Geophysical Research: Solid*
695 *Earth*, *120*(4), 2648–2671. https://doi.org/10.1002/2014JB011547

Wehbe, Y., Ghebreyesus, D., Temimi, M., Milewski, A., & Al Mandous, A. (2017). Assessment of the consistency among global precipitation products over the United Arab Emirates. *Journal of Hydrology: Regional Studies*, *12*, 122–135. https://doi.org/10.1016/j.ejrh.2017.05.002

Wei, L., Jiang, S., Ren, L., Wang, M., Zhang, L., Liu, Y., Yuan, F., & Yang, X. (2021). Evaluation of seventeen satellite-, reanalysis-, and gauge-based precipitation products for drought monitoring across mainland China. *Atmospheric Research*, *263*, 105813. https://doi.org/10.1016/j.atmosres.2021.105813

Wei, L., Jiang, S., Ren, L., Yuan, F., & Zhang, L. (2019). Performance of Two Long-Term Satellite-Based and GPCC 8.0 Precipitation Products for Drought Monitoring over the Yellow River Basin in China. *Sustainability*, *11*(18), 4969. https://doi.org/10.3390/su11184969

Wiese, D. N., Yuan, D.-N., Boening, C., Landerer, F. W., & Watkins, M. M. (2023). *JPL GRACE and GRACE-FO Mascon Ocean, Ice, and Hydrology Equivalent Water Height CRI Filtered. Ver. RL06.1Mv03.* [Dataset]. PO.DAAC, CA, USA. https://doi.org/10.5067/TEMSC-3JC63

Wu, X., Feng, X., Wang, Z., Chen, Y., & Deng, Z. (2023). Multi-source precipitation products assessment on drought monitoring across global major river basins. *Atmospheric Research*, *295*, 106982. https://doi.org/10.1016/j.atmosres.2023.106982

Xu, K., Yang, D., Yang, H., Li, Z., Qin, Y., & Shen, Y. (2015). Spatio-temporal variation of drought in China during 1961–2012: A climatic perspective. *Journal of Hydrology*, *526*, 253–264. https://doi.org/10.1016/j.jhydrol.2014.09.047